** ONLINE APPENDIX **

WANING IMMUNITY AND THE SECOND WAVE: SOME PROJECTIONS FOR SARS-CoV-2

Chryssi Giannitsarou* Stephen Kissler† Flavio Toxvaerd‡

*Faculty of Economics, University of Cambridge and CEPR. Email: cg349@cam.ac.uk.
†Harvard School of Public Health. Email: skissler@hsph.harvard.edu.
‡Faculty of Economics, University of Cambridge. Email: fmot2@cam.ac.uk.

A. Flow Chart of the SEIRS Model with Demographics

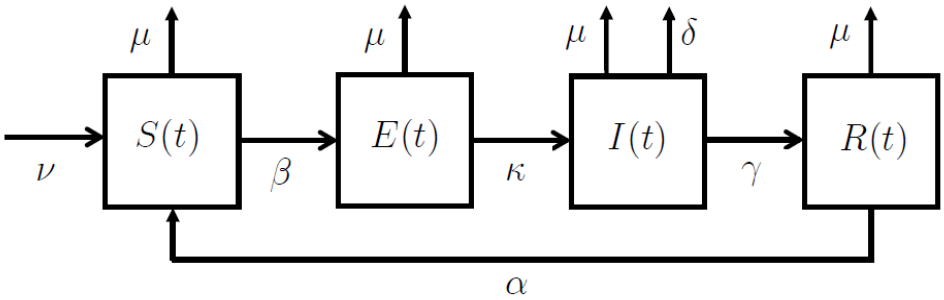

Figure 1: States and flows in the SEIRS model.

B. Tables

Parameter	**Value**	**Source**
ν	3.8/52	USA average 3.8 million births per year
μ	$1/(80 \times 52)$	USA life expectancy 80 years
γ	7/14	Kissler et al. (2020)
β	$\gamma \times 3$	Kissler et al. (2020)
κ	7/5	Kissler et al. (2020) and references therein
ε	1/2	Davies et al. (2020)
δ	$\gamma \times 0.0065$	IFR, various sources.
α	1/52	Kissler et al. (2020)
ρ	0.04/52	Standard yearly macro discount rate, 4%
y_S	1	Normalized to 1 unit of income
y_E	1	Equal to y_S
y_I	0.9	10% reduction in productivity due to infection
y_R	1	Equal to y_S
y	1	Income per person after T, equal to y_S
η	1	Quadratic costs
$\theta/2$	330×0.165	Aggregate income loss (Strong and Wellbourn, 2020)
T	100×52	Approximation of long/infinite horizon
N_0	330	US population, 330m
I_0	0.000033	1 in 10 m initially infected, Atkeson (2020)
E_0	$3 \times I_0$	Atkeson (2020)

Table 1: Parameter values for benchmark simulations.

	At the end of 6 years			At the end of horizon T		
$T = 100$ years	*Epi model*	*Econ model*	*Diff*	*Epi model*	*Econ model*	*Diff*
$IFR = 0.30\%,\ \alpha = 1/52$	4.496m	4.338m	158,010	61.744m	60.341m	1.403m
$IFR = 0.65\%,\ \alpha = 1/52$	**9.636m**	**8.212m**	**1.423m**	**123.440m**	**116.670m**	**6.767m**
$IFR = 1.20\%,\ \alpha = 1/52$	17.490m	14,174	17.476m	202.450m	351,920	202.100m
$IFR = 0.65\%,\ \alpha = 1/26$	16.716m	13,561	16.702m	206.140m	346,360	205.790m
$IFR = 0.65\%,\ \alpha = 1/52$	**9.636m**	**8.212m**	**1.423m**	**123.440m**	**116.670m**	**6.767m**
$IFR = 0.65\%,\ \alpha = 1/104$	5.764m	5.516m	248,120	69.296m	67.226m	2.070m
$IFR = 0.65\%,\ \alpha = 0$	2.061m	1.959m	102,120	3.280m	3.067m	213,590
$IFR = 0.65\%,\ \alpha = 1/52$				*Epi model*	*Econ model*	*Diff*
$T = 2$ years				3.852m	2.317m	1.535m
$T = 4$ years				6.784m	3.660m	3.123m
$T = 6$ years				9.636m	4.937m	4.699m

Table 2: Disease induced deaths for different scenarios. The benchmark case is highlighted in bold.

C. Long Run Dynamics of the Epidemic Model

The system of differential equations for the epidemic model is given by:

$$\dot{S} = \nu - \beta \frac{(I + \varepsilon E)\, S}{N} + \alpha R - \mu S, \tag{1}$$

$$\dot{E} = \beta \frac{(I + \varepsilon E)\, S}{N} - (\kappa + \mu)\, E, \tag{2}$$

$$\dot{I} = \kappa E - (\gamma + \delta + \mu)\, I, \tag{3}$$

$$\dot{R} = \gamma I - (\alpha + \mu)\, R, \tag{4}$$

$$\dot{N} = \nu - \mu N - \delta I. \tag{5}$$

We start by describing the basic reproductive rate $\mathcal{R}_0$, i.e. the number of secondary infectives per index case in a (naive) population of susceptibles.[1] Under the assumption that at the start of time the entire population is susceptible, the average number of new infections per infectious individual is determined by the transmission rate times the mean time that the exposed and infected individuals are infectious, i.e. by the following expression:

$$\mathcal{R}_0 = \frac{\kappa}{\kappa + \mu} \frac{\beta}{\gamma + \delta + \mu} + \frac{\varepsilon \beta}{\kappa + \mu}. \tag{6}$$

We note that the basic reproduction rate is independent of the waning immunity parameter α, because this parameter has no effect on how many infectives are generated per infectious individual.

To determine possible long run outcomes, we first note that in a long run steady state where population does not grow, we have that $\nu = \mu N^* + \delta I^*$. The model has two such steady states, the *disease-free steady state* and the *endemic steady state*. These can be recovered analytically as follows:

- **Disease-free steady state**: In this steady state $I^* = 0$ and $E^* = 0$. Then $N^* = \nu/\mu$ and $R^* = 0,\ S^* = \nu/\mu$.

- **Endemic steady state**: We require that $I^* \neq 0$, and assuming $\kappa \neq 0$ and $\alpha + \mu \neq 0$, then

$$E^* = \left(\frac{\gamma + \delta + \mu}{\kappa} \right) I^* \equiv \phi I^*, \tag{7}$$

$$R^* = \left(\frac{\gamma}{\alpha + \mu} \right) I^* \equiv \psi I^*. \tag{8}$$

From the first ODE by setting $\dot{S} = 0$, and substituting in the above we can show that

$$\frac{S^*}{N^*} = \frac{1}{\mathcal{R}_0}. \tag{9}$$

This means that in the endemic steady state of the SEIRS model with demographics (births and deaths), the proportion of susceptibles is inversely proportional to the basic reproduction rate $\mathcal{R}_0$.[2] With these expressions in place we can derive the population at the endemic steady

[1] This definition is taken from Keeling and Rohani (2008).

[2] Similar results can be shown for variations of such models with demographics, as explained in Keeling and Rohani (2008).

state to be

$$N^* = \nu \left(\frac{\delta}{1+\phi+\psi} \left(1 - \frac{1}{\mathcal{R}_0} \right) + \mu \right)^{-1} \tag{10}$$

and the following relations

$$\frac{E^*}{N^*} = \frac{\phi}{1+\phi+\psi} \left(1 - \frac{1}{\mathcal{R}_0} \right), \tag{11}$$

$$\frac{I^*}{N^*} = \frac{1}{1+\phi+\psi} \left(1 - \frac{1}{\mathcal{R}_0} \right), \tag{12}$$

$$\frac{R^*}{N^*} = \frac{\psi}{1+\phi+\psi} \left(1 - \frac{1}{\mathcal{R}_0} \right). \tag{13}$$

To analyze the stability of the two steady states, we derive the Jacobian of the system:

$$J(S,E,I,N) = \begin{bmatrix} -\beta\frac{(I+\varepsilon E)}{N} - (\alpha+\mu) & -\beta\varepsilon\frac{S}{N} - \alpha & -\beta\frac{S}{N} - \alpha & \beta\frac{(I+\varepsilon E)S}{N^2} - \alpha \\ \beta\frac{(I+\varepsilon E)}{N} & \beta\varepsilon\frac{S}{N} - (\kappa+\mu) & \beta\frac{S}{N} & -\beta\frac{(I+\varepsilon E)S}{N^2} \\ 0 & \kappa & -\kappa\phi & 0 \\ 0 & 0 & -\delta & -\mu \end{bmatrix}. \tag{14}$$

For the disease-free steady state, this becomes

$$J_{DF} = \begin{bmatrix} -(\alpha+\mu) & -\beta\varepsilon - \alpha & -\beta - \alpha & -\alpha \\ 0 & \beta\varepsilon - (\kappa+\mu) & \beta & 0 \\ 0 & \kappa & -\kappa\phi & 0 \\ 0 & 0 & -\delta & -\mu \end{bmatrix} \tag{15}$$

and for the endemic steady state, this becomes

$$J_E = \begin{bmatrix} -\beta\left(\frac{1+\varepsilon\phi}{1+\phi+\psi}\right)\left(1-\frac{1}{\mathcal{R}_0}\right) - (\alpha+\mu) & -\beta\varepsilon\frac{1}{\mathcal{R}_0} - \alpha & -\beta\frac{1}{\mathcal{R}_0} - \alpha & \beta\left(\frac{1+\varepsilon\phi}{1+\phi+\psi}\right)\left(1-\frac{1}{\mathcal{R}_0}\right)\frac{1}{\mathcal{R}_0} - \alpha \\ \beta\left(\frac{1+\varepsilon\phi}{1+\phi+\psi}\right)\left(1-\frac{1}{\mathcal{R}_0}\right) & \beta\varepsilon\frac{1}{\mathcal{R}_0} - (\kappa+\mu) & \beta\frac{1}{\mathcal{R}_0} & -\beta\left(\frac{1+\varepsilon\phi}{1+\phi+\psi}\right)\left(1-\frac{1}{\mathcal{R}_0}\right)\frac{1}{\mathcal{R}_0} \\ 0 & \kappa & -\phi\kappa & 0 \\ 0 & 0 & -\delta & -\mu \end{bmatrix}. \tag{16}$$

It can be shown that whenever $\mathcal{R}_0 < 1$, then the disease-free steady state is stable and the endemic steady state is unstable, while whenever $\mathcal{R}_0 > 1$, the disease-free steady state is unstable and the endemic steady state is stable. We can also confirm numerically that for our calibrated parameters and the ranges of parameters relevant for SARS-CoV-2, the disease-free steady state is unstable (i.e. at least one eigenvalue of J_{DF} has strictly positive real part) , while the endemic steady state is stable (i.e. all eigenvalues of J_E have strictly negative real parts). Importantly this is true for both $\alpha \neq 0$, i.e. for waning immunity and for $\alpha = 0$, i.e. for the SEIR model, for which immunity of individuals is permanent. Additionally, the endemic steady state exhibits damped oscillations (again irrespective of α), because J_E has eigenvalues that are conjugate complex.

The figures that follow show the uncontrolled disease dynamics in the following cases for short and long horizons for permanent immunity $\alpha = 0$ (Figure 2) and waning immunity $\alpha = 1/52$ (Figure 3). For all these, the initial condition of the population has now been set to the disease-free steady state $N^* = 304$ million people.

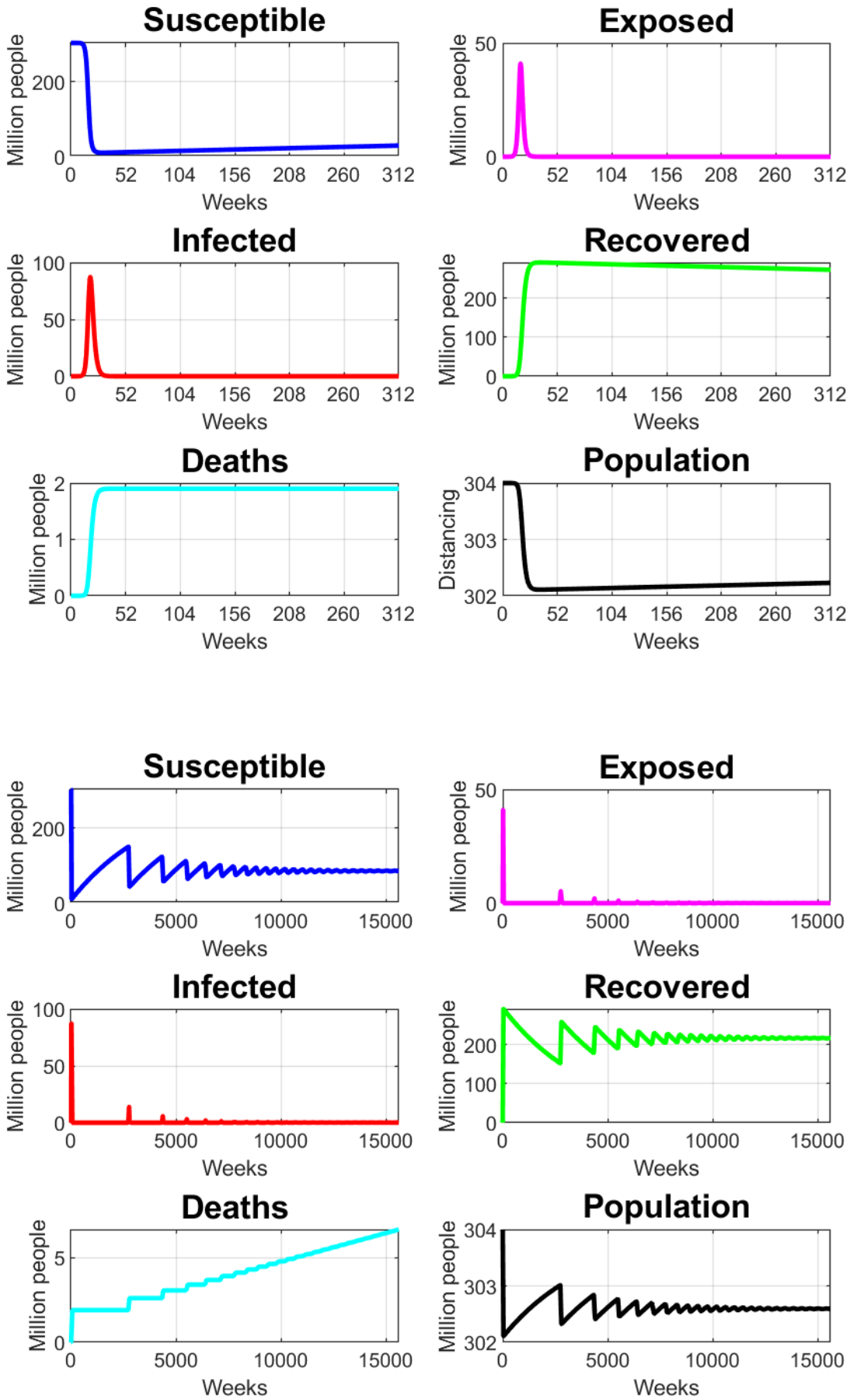

Figure 2: SEIR with demographics, uncontrolled dynamics. Top three rows show first six years, bottom three rows 300 years.

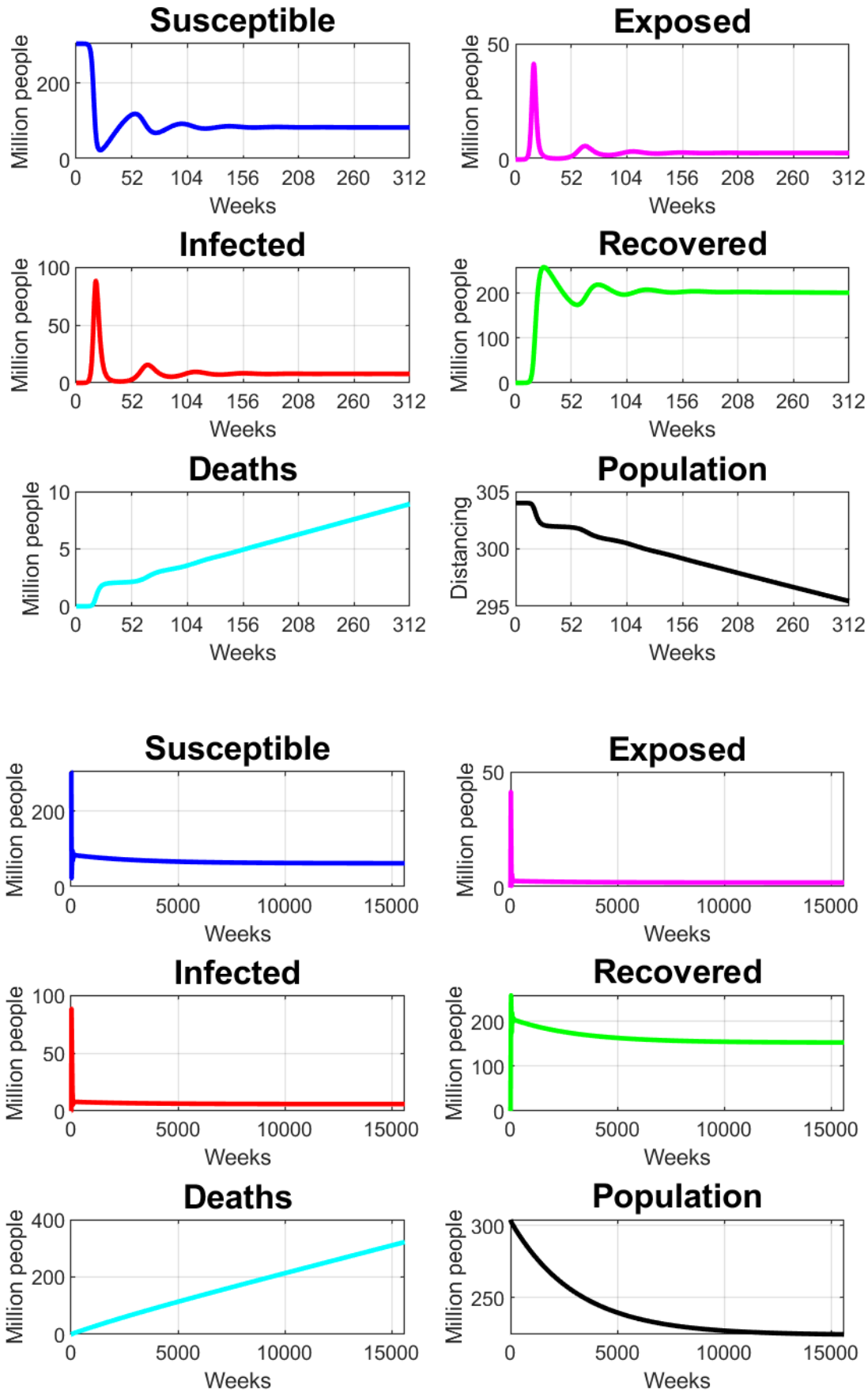

Figure 3: SEIRS with demographics, uncontrolled dynamics ($\alpha = 1/52$). Top three rows show first six years, bottom three rows 300 years.

D. Infectivity Reductions in the Epidemic Model

In the main analysis, we interpret the policy instrument d as some measure that reduces contacts between at-risk individuals and infectious individuals and we allow the social planner to vary this instrument at will over time. It is instructive to consider the dynamics of the model with some fixed value of d, which can be interpreted as other measures which reduce the infectiousness of the disease. For example, mass vaccination with incomplete vaccination coverage or with vaccines that only confer partial protection (as is the case with many vaccines) would effectively reduce the infectiousness parameter of the disease below the level β in such a manner.

Let the epidemic model now be described by

$$\dot{S} = \nu - (1-d)\beta\frac{(I+\varepsilon E)\,S}{N} + \alpha R - \mu S, \tag{17}$$

$$\dot{E} = (1-d)\beta\frac{(I+\varepsilon E)\,S}{N} - (\kappa+\mu)\,E, \tag{18}$$

$$\dot{I} = \kappa E - (\gamma+\delta+\mu)\,I, \tag{19}$$

$$\dot{R} = \gamma I - (\alpha+\mu)\,R, \tag{20}$$

$$\dot{N} = \nu - \mu N - \delta I, \tag{21}$$

where here we think of $d \in [0,1]$ as a *constant* parameter. The interpretation is the same as in the main part of the paper, i.e. that d is a way of reducing the contact rate between susceptibles and infectious individuals (exposed and infected) and can be loosely interpreted as a measure of social distancing. In this version of the model, the basic reproductive rate is given by

$$\tilde{\mathcal{R}}_0 = \frac{\kappa}{\kappa+\mu}\frac{\beta\,(1-d)}{\gamma+\delta+\mu} + \frac{\varepsilon\beta\,(1-d)}{\kappa+\mu}. \tag{22}$$

There are again two steady states, one endemic and one disease-free, and only one of them can be stable for each set of parameters. Specifically, if $\tilde{\mathcal{R}}_0 > 1$, then the endemic steady state is stable, while when $\tilde{\mathcal{R}}_0 < 1$ the disease-free steady state is stable. To link this with the original epidemic model, we note that the condition for the disease-free steady state to be stable is equivalent to requiring that

$$d > 1 - \frac{1}{\mathcal{R}_0} \equiv \tilde{d}, \tag{23}$$

where $\mathcal{R}_0$ is the rate of the basic epidemic model given in (6). This expression is very useful for understanding and interpreting the effects of the optimal social distancing policy: it shows that with enough social distancing (anything above a threshold $\tilde{d}$) it is possible to eradicate an otherwise endemic disease. As will be the case for some extreme parameterizations of the model, the social planner will optimally choose a long run social distancing policy that will be just about enough to tip the dynamics of the system towards the disease-free steady state. For which parameters this happens depends on the optimal control parameters, i.e. the cost of social distancing, the loss of income from those infected, the loss of lives, etc. For our benchmark calibration as given in Table 1, the value of this threshold is $\tilde{d} = 0.7154$.

E. Optimal Social Distancing Policy

The planner's problem is

$$\max_{d\in[0,1]}\left\{\int_0^T \exp\left(-\rho t\right)\left(y_S S\left(t\right)+y_E E\left(t\right)+y_I I\left(t\right)+y_R R\left(t\right)-\frac{\theta}{2}d^2\right)dt \right. \tag{24}$$
$$\left. +\int_T^\infty \exp\left(-\rho t\right) yN(t)dt\right\}.$$

The second integral, which represents the *scrap* or *salvage* value for the optimal control problem, is the integral from time T to infinity of the discounted value of the income generated by the total population, where the dynamics of the population are now determined by the ODE for N, but without the disease induced death rate. We assume that the income produced by each individual after T is y, and it satisfies $y = y_S$. That is,

$$V=\int_T^\infty \exp\left(-\rho t\right) N\left(t\right) ydt. \tag{25}$$

The ODE for population is $\dot{N}=\nu-\mu N$ and therefore its solution is

$$N\left(t\right)=\frac{\nu}{\mu}+C\exp\left(-\mu t\right), \tag{26}$$

where C is the constant to be determined by the size of the population at time T. For $N\left(T\right)$ at the start of the integral we have

$$N\left(T\right)=\frac{\nu}{\mu}+C\exp\left(-\mu T\right) \implies C=\left(N\left(T\right)-\frac{\nu}{\mu}\right)\exp\left(\mu T\right). \tag{27}$$

Therefore after T, the population evolves according to

$$N\left(t\right)=\frac{\nu}{\mu}+\left(N\left(T\right)-\frac{\nu}{\mu}\right)\exp\left(-\mu\left(t-T\right)\right), \text{ for } t\geq T. \tag{28}$$

With this in place we can now derive the scrap value to be

$$\begin{aligned} V &= \int_T^\infty y\exp\left(-\rho t\right)N\left(t\right)dt && (29)\\ &= \int_T^\infty y\exp\left(-\rho t\right)\left[\frac{\nu}{\mu}+\left(N\left(T\right)-\frac{\nu}{\mu}\right)\exp\left(\mu T\right)\exp\left(-\mu t\right)\right]dt && (30)\\ &= \exp\left(-\rho T\right)\left[\frac{\nu}{\rho\mu}+\left(N\left(T\right)-\frac{\nu}{\mu}\right)\frac{1}{\rho+\mu}\right]y. && (31)\end{aligned}$$

Therefore, the problem of the planner can be rewritten as

$$\max_{d\in[0,1]}\left\{\int_0^T \exp\left(-\rho t\right)\left(y_S S+y_E E+y_I I+y_R R-\frac{\theta}{2}d^2\right)dt \right. \tag{32}$$
$$\left. +\exp\left(-\rho T\right)\left[\frac{\nu}{\rho\mu}+\frac{1}{\rho+\mu}\left(N\left(T\right)-\frac{\nu}{\mu}\right)\right]y\right\}.$$

We start with the five differential equation constraints that describe the dynamics of the system:

$$\dot{S} = \nu - (1-d)\beta\left(I + \varepsilon E\right)\frac{S}{N} + \alpha R - \mu S, \tag{33}$$

$$\dot{E} = (1-d)\beta\left(I + \varepsilon E\right)\frac{S}{N} - \left(\kappa + \mu\right)E, \tag{34}$$

$$\dot{I} = \kappa E - \left(\gamma + \delta + \mu\right)I, \tag{35}$$

$$\dot{R} = \gamma I - \left(\alpha + \mu\right)R, \tag{36}$$

$$\dot{N} = \nu - \mu N - \delta I. \tag{37}$$

Because of the accounting equation, the social planner's problem can be reduced to one with only four differential equation constraints. We do so by eliminating R and substituting in $R = N - S - E - I$. The constraints thus become

$$\dot{S} = \nu + \alpha N - \left(\alpha + \mu\right)S - \alpha E - \alpha I - (1-d)\beta\left(I + \varepsilon E\right)\frac{S}{N}, \tag{38}$$

$$\dot{E} = (1-d)\beta\left(I + \varepsilon E\right)\frac{S}{N} - \left(\kappa + \mu\right)E, \tag{39}$$

$$\dot{I} = \kappa E - \left(\gamma + \delta + \mu\right)I, \tag{40}$$

$$\dot{N} = \nu - \mu N - \delta I. \tag{41}$$

Letting the costate variables for the constraints be denoted by λ_S, λ_E, λ_I and λ_N, the planner's Hamiltonian is given by

$$\begin{aligned} H \;=\; & e^{-\rho t}\left[\left(y_S - y_R\right)S + \left(y_S - y_R\right)E + \left(y_I - y_R\right)I + y_R N - \frac{\theta}{2}d^2\right] \\ & + \lambda_S\left[\nu + \alpha N - \left(\alpha + \mu\right)S - \alpha E - \alpha I - (1-d)\beta\left(I + \varepsilon E\right)\frac{S}{N}\right] \\ & + \lambda_E\left[(1-d)\beta\left(I + \varepsilon E\right)\frac{S}{N} - \left(\kappa + \mu\right)E\right] + \lambda_I\left[\kappa E - \left(\gamma + \delta + \mu\right)I\right] \\ & + \lambda_N\left(\nu - \mu N - \delta I\right). \end{aligned} \tag{42}$$

The first order condition with respect to d is

$$\frac{\partial H}{\partial d} = -e^{-\rho t}\theta d + \left(\lambda_S - \lambda_E\right)\beta\left(I + \varepsilon E\right)\frac{S}{N} = 0, \tag{43}$$

and therefore the optimal d must satisfy

$$d = \frac{e^{\rho t}}{\theta}\left(\lambda_S - \lambda_E\right)\beta\left(I + \varepsilon E\right)\frac{S}{N}. \tag{44}$$

Additionally, the optimal d^* must belong to the set of admissible controls, and since it is bounded and must satisfy $0 \leq d \leq 1$, it follows that:

$$d^* = \max\left\{0, \min\left\{1, \frac{e^{\rho t}}{\theta}\left(\lambda_S - \lambda_E\right)\beta\left(I + \varepsilon E\right)\frac{S}{N}\right\}\right\}. \tag{45}$$

A detailed explanation and derivations of how the maximum principle applies to bounded controls can be found in Lenhart and Workman (2007, ch. 7).

The laws of motion for the costate variables are given by

$$\dot{\lambda}_S = \lambda_S \left[\beta(1-d)\frac{(I+\varepsilon E)}{N} + \alpha + \mu\right] - \lambda_E \beta(1-d)\frac{(I+\varepsilon E)}{N} - e^{-\rho t}\left(y_S - y_R\right), \tag{46}$$

$$\dot{\lambda}_E = \lambda_S \left[\alpha + \beta\varepsilon(1-d)\frac{S}{N}\right] + \lambda_E \left[\kappa + \mu - (1-d)\beta\varepsilon\frac{S}{N}\right] - \kappa\lambda_I - e^{-\rho t}\left(y_S - y_R\right), \tag{47}$$

$$\dot{\lambda}_I = \left[\alpha + \beta\left(1-d\right)\frac{S}{N})\right]\lambda_S - \beta(1-d)\frac{S}{N}\lambda_E + \left(\gamma + \delta + \mu\right)\lambda_I + \lambda_N\delta - e^{-\rho t}\left(y_I - y_R\right), \tag{48}$$

$$\dot{\lambda}_N = -\lambda_S\alpha - \lambda_S(1-d)\beta\left(I+\varepsilon E\right)\frac{S}{N^2} + \lambda_E(1-d)\beta\left(I+\varepsilon E\right)\frac{S}{N^2} + \mu\lambda_N - e_R^{-\rho t}y_R. \tag{49}$$

Last, we also need the following transversality conditions to be satisfied:

$$\lambda_S\left(T\right) = \lambda_E\left(T\right) = \lambda_I\left(T\right) = 0 \tag{50}$$

and the last transversality condition equates λ_N to the derivative with respect to $N(T)$ of the term

$$\int_T^\infty e^{-\rho t}N(t)ydt = \exp\left(-\rho T\right)\left[\frac{\nu}{\rho\mu} + \frac{1}{\rho+\mu}\left(N\left(T\right) - \frac{\nu}{\mu}\right)\right]y. \tag{51}$$

This yields

$$\lambda_N\left(T\right) = \exp\left(-\rho T\right)\frac{y}{\rho+\mu}. \tag{52}$$

We should point out that the conditions (43), (46), (47), (48), (49), (50) and (52) are necessary for optimality but not sufficient. This stems from the fact that the Hamiltonian (42) is non-concave in the state variables. For this type of problem, neither Mangasarian nor Arrow type sufficiency conditions apply and alternative methods must be used to verify the optimality of a given candidate path.[3] These typically rely on characterizing paths that satisfy the necessary conditions in a neighborhood of multiple steady states and then directly computing and comparing value functions for any regions of the state space in which those multiple paths overlap. In our simulations, we characterize the trajectory of state and costate variables that satisfies the necessary Hamiltonian and transversality conditions. As we have shown, for every parametrization the model exhibits two steady states, of which only one is stable. Moreover, for the parameterizations that we have worked with, we have found no instances of multiple equilibrium paths that satisfy the necessary conditions for optimality.

F. Numerical Solution Method

To solve the model numerically, we use a forward-backward sweep method as described in detail in Lenhart and Workman (2007, ch. 4 and 12). We outline the method here and provide the details of the numerical setup used for generating the figures in the paper.

First, the time interval $[0, T]$ is split into equal intervals each of which has length $h < 1$, and using this time gird of $M+1$ points, the continuous time state and costate variables are approximated with vectors of length $M+1$. The algorithm for finding the optimal policy involves the following steps:

- **Step 1**: Set initial guess for $[d_1, ..., d_{M+1}]$, typically set to zeros.

[3] Brock and Dochert (1983) introduced the generalized maximum principe in the context of growth models, while Brock and Starrett (2003) applied this technique to shallow lake systems. Deissenberg et al. (2004) contains an excellent synthesis of this literature. Rowthorn and Toxvaerd (2020) apply these techniques to the optimal control of disease dynamics.

- **Step 2**: Use initial conditions for $N_1 \equiv N(0)$, $S_1 \equiv S(0)$, $E_1 \equiv E(0)$ and $I_1 \equiv I(0)$ as determined by the model calibration and solve forward in time the system of differential equations (38)-(41), using a 4th order Runge-Kutta forward sweep.

- **Step 3**: Use the transversality conditions (50) and (52), i.e. the costates evaluated at time T, the current vector of d, and the vector of state variables from Step 2, to solve backward in time the system of differential equations (46)-(49), using a 4th order Runge-Kutta backward sweep.

- **Step 4**: Use the current vector of states (from Step 2) and costates (from Step 3) to evaluate d_{new} using (45). Update d using a convex combination of the old and new d, using an updating 'gain' parameter $0 < g < 1$:
$$d = g * d_{new} + (1 - g) * d_{old} \tag{53}$$

- **Step 5**: Iterate until convergence according to a required tolerance level $toler$.

Our results and graphs were generated using the following specifications: First, we use $h = 1/10$. For the smallest time interval we work with, i.e. $T = 104$ weeks, this implies a grid of more than 1,000 points, which is sufficient for a good approximation. We have also tried values of $h = 1/50$ and $h = 1/100$ and found that the improvements in precision are insignificant. Since a larger number of grid points greatly increases computational time, we kept 1/10 as our benchmark value for h.

Second, we use an updating gain parameter of $g = 0.01$ for almost all simulations, apart from a few simulations with high δ, or high α, and/or large (approximately infinite) time T. The smallest updating gain we used was $g = 0.0005$. Smaller gain improves the stability of the algorithm, but increases the computing time considerably.

Third, for the convergence of the '*while*' loop we use tolerance level $tol = 1e - 13$. Requiring tight tolerance for the numerical simulations is very important for good accuracy of the algorithm because of the control bounds. If the tolerance is wide, then the algorithm may 'converge' too quickly and produce solutions that are on the lower or upper bound of the control (i.e. at 0 or 1) for most of the time horizon, and which are *not* optimal.

Fourth, for most of our simulations, our approximation of a very long horizon is done by setting $T = 100$ years. For 'infinite' horizon approximations we discard the last 200-400 weeks to avoid end-of-horizon distortions. The Matlab code for the simulations is provided on the corresponding author's website.

G. Optimal Social Distancing in SEIR Without Demographics

The following two figures show the dynamics and optimal policy for the SEIR model (i.e. permanent immunity) in (a) the benchmark case, i.e. with natural births and deaths, and (b) in a version without demographics, i.e. $\nu = \mu = 0$, both showing the first six years of simulations for $T = 100$ years. We note that the main differences between these sets of plots are quantitative rather than qualitative. Notably, optimal social distancing is significantly higher when a closed population is considered. Intuitively, when the population is not replenished by new births, each individual life receives a much higher weight in the planner's objective and hence there is a much stronger need to avoid infections. Disregarding demographics may thus lead to policy recommendations that inflate the need for disease control, relative to the model with population turnover.

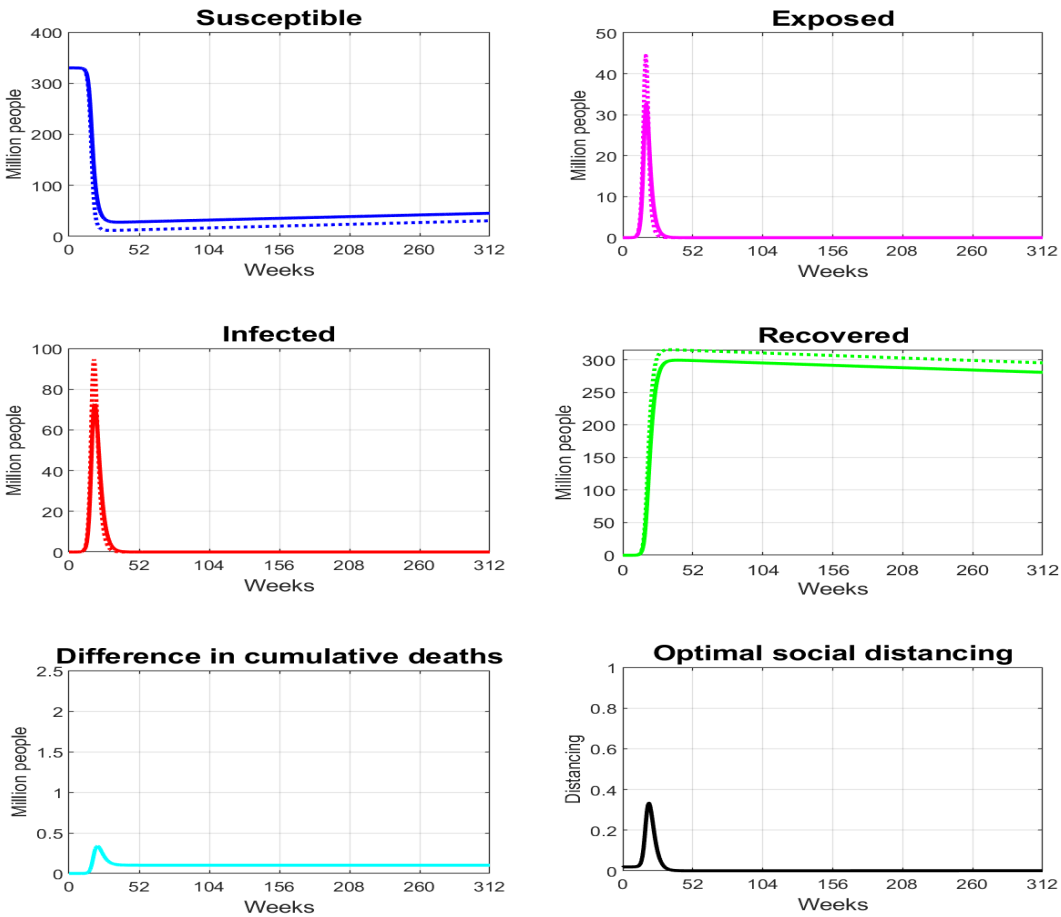

Figure 4: *SEIR model with demographics.* Benchmark values 3.8 million births per year and life expectancy of 80 years. Dotted line is uncontrolled (epidemic) model and solid line under optimal social distancing policy.

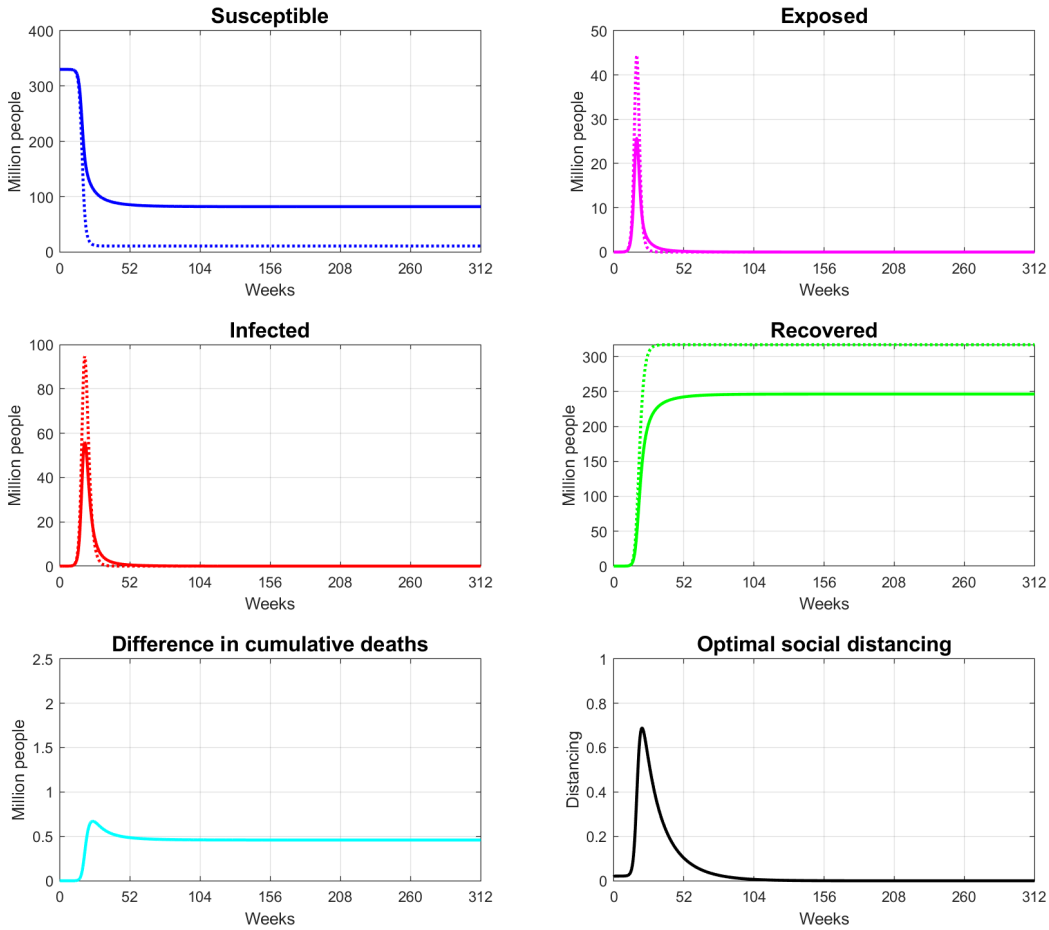

Figure 5: *SEIR model without demographics* ($\nu = \mu = 0$). Dotted line is uncontrolled (epidemic) model and solid line under optimal social distancing policy.

References

[1] Alvarez, F., D. Argente and F. Lippi (2020). A Simple Planning Problem for COVID-19 Lockdown, *NBER Working Paper* 26981.

[2] Armstrong, Gregory L., Laura A. Conn and Robert W. Pinner (1999). Trends in Infectious Disease Mortality in the United States During the 20th Century, *Journal of the Americal Medical Association*, 281(1), 61-66.

[3] Atkeson, A. (2020). What Will Be the Economic Impact of COVID-19 in the US? Rough Estimates of Disease Scenarios, *NBER Working Paper* 26867.

[4] Brauer, F. and C. Castillo-Chavez (2012). Mathematical Model in Population Biology and Epidemiology, *Springer*.

[5] Brock, W. A. and D. Starrett (2003): Managing Systems with Non-convex Positive Feedback, *Environmental and Resource Economics*, 26(4): 575-602.

[6] Brock, W. A. and W. D. Dochert (1983). The Generalized Maximum Principle, *Social Systems Research Institute Workshop Series*, University of Wisconsin.

[7] Callow, K. A., H. F. Parry, M. Sergeant and D. A. Tyrrell (1990). The Time Course of the Immune Response to Experimental Coronavirus Infection of Man, *Epidemiology and Infection*, 105(2), 435–446. doi: 10.1017/s0950268800048019.

[8] Davies, N.G., P. Klepac, Y. Liu, et al. (2020). Age-Dependent Effects in the Transmission and Control of COVID-19 Epidemics, *Nature Medicine* 26, 1205-1211. https://doi.org/10.1038/s41591-020-0962-9.

[9] Davies, N.G., P. Klepac, Y. Liu, K. Prem, M. Jit, CMMID COVID-19 working group, R. M. Eggo (2020). Age-Dependent Effects in the Transmission and Control of COVID-19 Epidemics, unpublished manuscript, medRxiv doi: https://doi.org/10.1101/2020.03.24.20043018.

[10] Deissenberg, C., G. Feichtinger, W. Semmler and F. Wirl (2004). Multiple Equilibria, History Dependence and Global Dynamics in Intertemporal Optimization Problems, in Barnett et al. (2004). Economic Complexity, Non-Linear Dynamics, Multi-Agents Economies, and Learning, International Symposia in Economic Theory and Econometrics, *Elsevier*.

[11] Eichenbaum, M., S. Rebelo and M. Trabrandt (2020). The Macroeconomics of Epidemics, *NBER Working Paper* 26882.

[12] Galanti, M. and J. Shaman (2020). Direct observation of repeated infections with endemic coronaviruses, *Journal of Infectious Diseases*, doi:10.1093/infdis/jiaa392.

[13] Grassly, Nicholas C., Christophe Fraser and Geoffrey P. Garnett (2005). Host Immunity and Synchronized Epidemics of Syphilis Across the United States, *Nature*, 433, 417-421.

[14] Greer, Meredith, Raj Saha, Alex Gogliettino, Chialin Yu and Kyle Zollo-Venecek (2020). Emergence of Oscillations in a Simple Epidemic Model with Demographic Data, *Royal Society Open Science*, 7(1), https://doi.org/10.1098/rsos.191187.

[15] Grenfell, B. T., O. N. Bjørnstad and J. Kappey (2001). Travelling Waves and Spatial Hierarchies in Measles Epidemics, *Nature*, 414, 716-723.

[16] Grenfell, Bryan and Ottar Bjørnstad (2005). Epidemic Cycling and Immunity, *Nature*, 433, 366-367.

[17] Gudbjartsson, D.F., G.L. Norddahl and P. Melsted et al. (2020). Humoral Immune Response to SARS-CoV-2 in Iceland, *The New England Journal of Medicine,* DOI: 10.1056/NEJMoa2026116.

[18] Hall, R. E., C. Jones and P. Klenow (2020). Trading Off Consumption and COVID-19 Deaths. *Federal Reserve Bank of Minneapolis, Quarterly Review*, 42(1).

[19] Hansen, Victoria, Eyal Oren, Leslie K. Dennis and Heidi E. Brown (2016). Infectious Disease Mortality Trends in the United States, 1980-2014, *Journal of the Americal Medical Association*, 316(20), 2149-2151.

[20] Kaplan, G., B. Moll and G. Violante (2020). The Great Lockdown and the Big Stimulus: Tracing the Pandemic Possibility Frontier for the U.S., *CEPR Discussion Paper 15256.*

[21] Keeling, Matt J. and Pejman Rohani (2008). Modeling Infectious Diseases, *Princeton University Press.*

[22] Kissler, S. M., C. Tedijanto, E. Goldstein, Y. H. Grad and M. Lipsitch (2020). Projecting the Transmission Dynamics of SARS-CoV-2 through the Postpandemic Period, *Science*, 368 (6493), 860–686. doi: 10.1126/science.abb5793

[23] Krueger, D., H. Uhlig and T. Xie (2020). Macroeconomic Dynamics and Reallocation in an Epidemic, *NBER Working Paper* 27047.

[24] Lenhart, S. and J. T. Workman (2007). Optimal Control Applied to Biological Models. Mathematical and Computational Biology Series, *Chapman & Hall/CRC*, London.

[25] Li, R., S. Pei, B. Chen, Y. Song, T. Zhang, W. Yang, and J. Shaman (2020). Substantial undocumented infection facilitates the rapid dissemination of novel coronavirus (SARS-CoV-2). Science, 368 (6490), 489-493. doi: 10.1126/science.abb3221

[26] Meyerowitz-Katz, G. and L. Merone (2020). A systematic review and meta-analysis of published research data on COVID-19 infection-fatality rates, medRxiv 2020.05.03.20089854; doi: https://doi.org/10.1101/2020.05.03.20089854.

[27] Mo, H., Zeng, G., Ren, X., Li, H., Ke, C., Tan, Y., Cai, C., Lai, K., Chen, R., Chan-Yeung, M. And Zhong, N. (2006), Longitudinal profile of antibodies against SARS-coronavirus in SARS patients and their clinical significance. *Respirology*, 11: 49-53. doi:10.1111/j.1440-1843.2006.00783.x

[28] Javier Perez-Saez, Stephen A Lauer, Laurent Kaiser, Simon Regard, Elisabeth Delaporte, Idris Guessous, Silvia Stringhini, Andrew S Azman, et al. (2020). Serology-informed estimates of SARS-CoV-2 infection fatality risk in Geneva, Switzerland, *The Lancet Infectious Diseases*, ISSN 1473-3099, https://doi.org/10.1016/S1473-3099(20)30584-3.

[29] Payne, D. C., Iblan, I., Rha, B., et al. (2016). Persistence of Antibodies against Middle East Respiratory Syndrome Coronavirus. *Emerging Infectious Diseases*, 22(10), 1824-1826. https://dx.doi.org/10.3201/eid2210.160706.

[30] Rachel, Łukasz (2020): The Second Wave, *mimeo.*

[31] Rowthorn, R. and F. Toxvaerd (2020). The Optimal Control of Infectious Diseases Via Prevention and Treatment, *Cambridge-INET Working Paper Series* No: 2020/13.

[32] Salje, H., C. Tran Kiem, N. Lefrancq, N. Courtejoie, P. Bosetti, J. Paireau, A. Andronico, N. Hoze, J. Richet, C-L. Dubost, Y. Le Strat, J. Lessler, D. Levy-Bruhl, A. Fontanet, L. Opatowski, P-Y. Boelle, S. Cauchemez (2020). Estimating the burden of SARS-CoV-2 in France, *Science*, 13 May 2020, doi: 10.1126/science.abc3517.

[33] Seow, J., C. Graham, B. Merrick et al. (2020). Longitudinal evaluation and decline of antibody responses in SARS-CoV-2 infection. Unpublished manuscript, medRxiv 2020.07.09.20148429; doi: https://doi.org/10.1101/2020.07.09.20148429.

[34] Strong, A. and J. W. Welburn (2020). An Estimation of the Economic Costs of Social-Distancing Policies, Research Report RR-A173-1, *RAND Corporation.*

[35] Swanson, D. and R. Cossman (2020). A Simple Method for Estimating the Number of Unconfirmed COVID-19 Cases in a Local Area that Includes a Confidence Interval: A Case Study of Whatcom County, Washington, unpublished manuscript, medRxiv, doi: 10.1101/2020.04.30.20086181.

[36] To, K. K. W, I. Fan-Ngai Hung, J. D. Ip, et al. (2020). COVID-19 re-infection by a phylogenetically distinct SARS-coronavirus-2 strain confirmed by whole genome sequencing, *Clinical Infectious Diseases*, https://doi.org/10.1093/cid/ciaa1275.

[37] Toxvaerd, F. (2019). Rational Disinhibition and Externalities in Prevention, *International Economic Review*, 60(4), 1737-1755.

[38] Toxvaerd, F. (2020). Equilibrium social Distancing, *Cambridge-INET Working Paper Series* No: 2020/08.

[39] Verity, R., L. C. Okell, I. Dorigatti, P. Winskill, C. Whittaker, N. Imai, G. Cuomo-Dannenburg, H. Thompson, P. G. T. Walker, H. Fu, A. Dighe, J. T. Griffin, M. Baguelin, S. Bhatia, A. Boonyasiri, A. Cori, Z. Cucunube, R. FitzJohn, K. Gaythorpe, W. Green, A. Hamlet, W. Hinsley, D. Laydon, G. Nedjati-Gilani, S. Riley, S. van Elsland, E. Volz, H. Wang, Y. Wang, X. Xi, C. A. Donnelly, A. C. Ghani, N. M. Ferguson (2020). Estimates of the Severity of Coronavirus Disease 2019: A Model-Based Analysis, *The Lancet Infectious Diseases*, 20(6), 669-677, https://doi.org/10.1016/S1473-3099(20)30243-7.